

# GLUEBALL REGGE TRAJECTORIES IN (2+1) DIMENSIONAL GAUGE THEORIES

Harvey B. Meyer<sup>1</sup>, Michael J. Teper<sup>2</sup>

Theoretical Physics, University of Oxford, 1 Keble Road,  
Oxford, OX1 3NP, United Kingdom

**Abstract.-** We compute glueball masses for even spins ranging from 0 to 6, in the  $D = 2 + 1$   $SU(2)$  lattice gauge theory. We do so over a wide range of lattice spacings, and this allows a well-controlled extrapolation to the continuum limit. When the resulting spectrum is presented in the form of a Chew-Frautschi plot we find that we can draw a straight Regge trajectory going through the lightest glueballs of spin 0, 2, 4 and 6. The slope of this trajectory is small and turns out to lie between the predictions of the adjoint-string and flux-tube glueball models. The intercept we find,  $\alpha_0 \sim -1$ , is much lower than is needed for this leading trajectory to play a ‘Pomeron-like’ role of the kind it is often believed to play in  $D = 3 + 1$ . We elaborate the Regge theory of high energy scattering in 2 space dimensions, and we conclude, from the observed low intercept, that high-energy glueball scattering is not dominated by the leading Regge pole exchange, but rather by a more complex singularity structure in the region  $0 \leq \text{Re}\lambda \leq \frac{1}{2}$  of the complex angular momentum  $\lambda$  plane. We show that these conclusions do not change if we go to larger groups,  $SU(N > 2)$ , and indeed to  $SU(\infty)$ , and we contrast all this with our very preliminary calculations in the  $D=3+1$   $SU(3)$  gauge theory.

---

<sup>1</sup>meyer@thphys.ox.ac.uk

<sup>2</sup>teper@thphys.ox.ac.uk

# 1 Introduction

On a Chew-Frautschi plot ( $J$  versus  $m^2$ ) the experimentally observed mesons and baryons appear to lie on (nearly) linear and parallel Regge trajectories,  $J = \alpha_0 + \alpha' m^2$ , with the exchange of the corresponding Regge poles (normally) dominating any high energy scattering that involves the exchange of non-trivial quantum numbers [1]. The total cross-section, on the other hand, is related by unitarity to forward elastic scattering and this is dominated by the ‘Pomeron’ which carries vacuum quantum numbers [1, 2, 3]. The Pomeron trajectory is qualitatively different from other Regge trajectories in that it appears to be much flatter ( $\alpha'$  much smaller) and it is not clear what physical particles correspond to integer values of  $J$ . There are long-standing speculations that these might be glueballs. Thus if one were to calculate the mass spectrum of the  $SU(3)$  gauge theory one could investigate whether the glueball masses fall on linear trajectories and whether these trajectories have the properties of the Pomeron.

Of course one does not expect the leading glueball trajectory to be exactly like the Pomeron since in the real world there will be mixing between glueballs and flavour-singlet  $q\bar{q}$  mesons; just as the usual meson/baryon trajectories cannot be exactly linear because the higher- $J$  mesons are unstable. It is only in the limit of  $SU(N \rightarrow \infty)$  that one can expect exactly linear trajectories (no decays) and the leading glueball Regge trajectory to be the Pomeron (no mixing). However there are good heuristic arguments to believe that  $QCD_{N=3}$  is close to  $QCD_{N=\infty}$  [4], and lattice calculations support this idea to the extent that they have shown that for pure gauge theories even  $N = 2$  is ‘close to’  $N = \infty$  [5].

Although it is now easy to calculate the lightest masses of a pure gauge theory using lattice Monte Carlo simulations, calculating masses of higher  $J$  states is more subtle because a cubic lattice respects only a small subgroup of the full rotation group and each representation of this subgroup contains states that correspond to different  $J$  in the continuum limit. This difficulty is compounded by the fact that the higher  $J$  states, being heavier, are more difficult to calculate accurately. In a recent paper [6] we have developed techniques for identifying states of arbitrary  $J$  on a lattice and we are now in the process of applying these techniques to determine if glueballs fall on linear Regge trajectories and if so whether the leading trajectory has the characteristics of the Pomeron.

In this paper we address this question in the context of the  $D = 2 + 1$   $SU(2)$  gauge theory. At first glance this may seem far removed from the case that is of immediate physical interest,  $SU(3)$  in  $D = 3 + 1$ , but the fact that the computations are much faster in  $D = 2 + 1$  than in  $D = 3 + 1$  means that we can expect to obtain more accurate results, more quickly, and so test the efficiency of our approach. Moreover, at closer inspection, one finds that  $D = 2 + 1$  non-Abelian gauge theories resemble those in  $D = 3 + 1$  in a number of relevant respects. They become free at short distances, the coupling sets the dynamical length scale, and the (dimensionless) coupling becomes strong at large distances. They are linearly confining, and the confining flux tube appears to behave like a simple bosonic string at large distances [7]. The light glueball spectrum more-or-less fits the expectations of a flux loop model, just as it does in 3+1 dimensions [8, 9, 10]. Moreover, as we shall see below, the same simple models that serve to predict linear glueball Regge trajectories in  $D = 3 + 1$ , predict their existence in the case of  $D = 2 + 1$ . We also note that the link to string theories (at least at large  $N$ ) can be made in  $D = 2 + 1$  just as in  $D = 3 + 1$  [13]. For all these reasons we believe that our exercise is of significant theoretical interest.

At a more heuristic level, one is motivated to search for a Pomeron trajectory where one has

high energy cross sections that are roughly constant in energy. Although the scattering of glueballs has not been observed experimentally, one's intuition is that they will behave as 'black discs', just like the usual mesons and hadrons, and so it makes sense to speculate that the Pomeron might be the leading (glueball) Regge trajectory in the  $D=3+1$   $SU(3)$  gauge theory. We do not expect this to depend strongly on the number of colours, so it should be a property of all  $SU(N)$  gauge theories. Finally, since we can think of no obvious reason why going from 3 to 2 spatial dimensions should prevent colliding glueballs from having roughly constant cross-sections at high energies – although as 'black segments' rather than as 'black discs' – we believe it makes sense to search for something like the Pomeron in  $D=2+1$   $SU(N)$  gauge theories.

Although our primary aim here is to see if we can learn something about the Pomeron from our lattice glueball calculations, the fact is that our results can also be used both to test models and to test the accuracy of approximate analytic calculations. An example of the former is the flux loop model for glueballs [8] which has recently been compared to the low- $J$  glueball mass spectrum of  $D = 2 + 1$   $SU(N)$  gauge theories [10]. An example of the latter is transverse lattice light front quantisation [11]. (Which has some problems similar to ours in determining states of arbitrary  $J$ .) Another example is the conjectured duality between supergravity and large  $N$  gauge theories [12] and its generalisation to the non-supersymmetric case [13]. Extensive quantitative calculations have been undertaken [14] to compute glueball masses in  $(2+1)$  and  $(3+1)$  dimensions using the AdS/CFT correspondence. The spectra corresponding to the quantum numbers  $2^{++}$ ,  $1^{+-}$ ,  $1^{--}$ ,  $0^{++}$ ,  $0^{--}$  and  $0^{-+}$  have been computed. It would be interesting to have a computation of the higher spin states in order to compare them to the new lattice data and to see if they lie on straight Regge trajectories. That would require the inclusion of stringy corrections to the low-energy effective action. However, because these higher spin states derive from string dynamics, one can expect them to lie on straight Regge trajectories.

The contents of this paper are as follows. In the next section we remind the reader of two simple, but plausible, models for glueballs in  $3+1$  dimensions and show how they directly carry over into  $2+1$  dimensions where they also predict linear Regge trajectories with small slopes. In the following section we discuss high energy scattering. We begin by showing how Regge theory can be applied in two space dimensions (with the details relegated to Appendices A and B). We then turn to perturbative Pomeron calculations, where there has been a great deal of work during the last decade, and investigate what happens when one moves from 3 to 2 space dimensions. Here we start with the old Low model, and the more recent dipole-dipole scattering approach, then we move on to the issue of gluon Reggeisation and finish with the BFKL Pomeron. Having established the general theoretical and phenomenological background to the problem, we turn to our lattice calculation of how glueball masses increase with their spin  $J$ . The calculation is novel in two respects. Firstly one has to surmount the problems posed by the limited rotational invariance of a square lattice. This we do using the techniques recently developed in [6]. Secondly, the fact that the higher- $J$  glueball masses are considerably heavier makes it difficult to calculate their masses from Euclidean correlators. Here we use a multi-level algorithm recently developed in [15], which extends to glueballs earlier work [16] for Polyakov loops. Using these techniques we obtain quite accurate continuum extrapolations of the  $J = 0, 2, 4, 6$  glueball masses. We find that the lightest glueballs of even  $J$  lie on a linear trajectory in a Chew-Frautschi plot of  $J$  versus  $m^2$ , and that the slope is small just as one would expect for a Pomeron pole. However the intercept is much too

low to provide a constant high energy cross-section, and we discuss the physical implications of this result. Finally we present some results for the leading glueball trajectory in  $SU(N > 2)$  gauge theories, showing that there is no qualitative change as  $N$  varies from 2 to  $\infty$ .

We conclude with a summary, a discussion of how our calculations should be improved upon, and a mention of the preliminary results we have obtained in a similar study of the quenched 3+1 dimensional  $SU(3)$  theory.

## 2 Glueball models and the large $J$ limit

In the standard valence quark picture, a high  $J$  meson will consist of a  $q$  and  $\bar{q}$  rotating rapidly around their common centre of mass. For large  $J$  they will be far apart and the chromoelectric flux between them will be localised in a flux tube which also rotates rapidly, and so contributes to  $J$ . In a generic model of such a system (see e.g. [17]) a simple calculation (that we shall repeat below) shows that the spin and mass are related linearly,  $J = \alpha_0 + \alpha' M^2$ , and that the slope is related to the tension  $\sigma_f$  of the confining string as  $\alpha' = 1/2\pi\sigma_f$ . (The subscript  $f$  indicates that the charges and flux are in the fundamental representation. We will often follow convention and use  $\sigma \equiv \sigma_f$  instead.) If one uses a phenomenologically sensible value for  $\sigma_f$  one obtains a value of  $\alpha'$  very similar to that which is experimentally observed for meson trajectories. This picture might well become exact in the large- $N$  limit where the fundamental string will not break and all the mesons are stable.

This picture can be generalised directly to glueballs. We have two rotating gluons joined by a rotating flux tube that contains flux in the adjoint rather than fundamental representation. This is the first model we consider below. However for glueballs there is another possibility that is equally natural: the glueballs may be composed of closed loops of fundamental flux. This is the second model we consider. The first model is natural in a valence gluon approach, while the second arises naturally in a string theory. They are not exclusive; both may contribute to the glueball spectrum. Indeed if there are two classes of glueball states, each with its own leading Regge trajectory, then this might provide an explanation for why experimentally there appear to be two distinct Pomeron trajectories, the hard ‘Pomeron’ and the ‘soft’ Pomeron [3]. However such speculations belong to  $D = 3 + 1$  rather than to the  $D = 2 + 1$  gauge theories that we analyse in this paper. What is interesting for our purposes is that both models can be motivated as easily in  $D = 2 + 1$  as in  $D = 3 + 1$  and in both cases predict (see below) linear glueball trajectories with some Pomeron-like properties.

### 2.1 Adjoint string model

In this model a high- $J$  glueball is imagined to be composed of two gluons joined by a ‘string’ in the adjoint representation, with the whole system rotating rapidly. This is a direct extension to glueballs of the usual model for high- $J$   $q\bar{q}$  mesons where the  $q$  and  $\bar{q}$  are joined by a ‘string’ in the fundamental representation. The adjoint string is of course unstable, once it is long enough (as it will be at high  $J$ ), but this is also true of the fundamental string in QCD. What is important for the the model to make sense is that the decay width should be sufficiently small. (Essentially that the lifetime of the adjoint string should be much longer than the period of rotation.) In  $SU(N)$  gauge

theories, both the adjoint and fundamental strings become completely stable as  $N \rightarrow \infty$ . So if we are close to that limit the model should make sense. Since adjoint string breaking in  $SU(N)$  occurs at  $O(1/N^2)$  while fundamental string breaking in  $QCD_N$  occurs at  $O(1/N)$ , one would expect the instability to be less of a problem in the former case. Moreover there is now considerable evidence [18, 19, 20] from lattice calculations that the  $D = 3 + 1$   $SU(3)$  gauge theory is indeed ‘close’ to  $SU(\infty)$ , and that this is also the case for the  $D = 2 + 1$   $SU(2)$  gauge theory [5].

The calculation of how  $J$  varies with the mass  $M$  of the glueball is exactly as for the  $q\bar{q}$  case [17]. That is to say, we consider the string joining the two gluons as a rigid segment of length  $2r_0$ , rotating with angular momentum  $J$  (the contribution of the valence gluons being negligible at high enough  $J$ ). The local velocity at a point along the segment is thus  $v(r) = r/r_0$  (one maximises  $J$  at given  $M$  if the end-points move with the speed of light), so that

$$M = 2 \int_0^{r_0} \frac{\sigma_a dr}{\sqrt{1 - v^2(r)}} = \sigma_a \pi r_0 \quad (1)$$

$$J = 2 \int_0^{r_0} \frac{\sigma_a r v(r) dr}{\sqrt{1 - v^2(r)}} = \frac{\pi}{2} \sigma_a r_0^2, \quad (2)$$

and, eliminating  $r_0$ ,

$$J = \frac{M^2}{2\pi\sigma_a} \quad (3)$$

we obtain a linear Regge trajectory of slope  $\alpha'_{AS} = \frac{1}{2\pi\sigma_a}$  where  $\sigma_a$  is the adjoint string tension. So this model predicts that the slope of the leading glueball trajectory is smaller than that of the leading meson trajectory by a factor  $\sigma_a/\sigma_f$ . For  $SU(3)$  we know that  $\sigma_a \simeq 2.25\sigma_f$  [21], so the leading glueball trajectory will have a slope  $\alpha'_{AS} \sim 0.88/2.25 \sim 0.39 \text{ GeV}^{-2}$  if we input the usual Regge slope of about  $\alpha'_R = \frac{1}{2\pi\sigma_f} \simeq 0.88 \text{ GeV}^{-2}$ . This is only a little larger than the actual slope of the Pomeron. Thus to this extent the model is consistent with the idea that the Pomeron is the leading glueball trajectory, perhaps modified by mixing with the flavour-singlet meson Regge trajectory. Unfortunately the model cannot predict the intercept  $\alpha_0$  of the trajectory, because it is valid at best at large  $J$ .

Since in this model the rotating glueball lies entirely within a plane, the calculation is identical for  $D = 2 + 1$  and  $D = 3 + 1$ , as indeed is the motivation for the applicability of the model. Thus it is a plausible model for the leading Regge trajectory in the  $D = 2 + 1$   $SU(2)$  gauge theory that we investigate in this paper. The only difference is that in  $SU(2)$  one expects  $\sigma_a \simeq 8\sigma_f/3$  and hence an even flatter trajectory than in  $SU(3)$ .

The above simple classical calculation can be made more rigorous in an effective Hamiltonian approach; see [1] for a review. There the calculation is for  $D = 3 + 1$ , but the main conclusion remains the same in  $2+1$  dimensions.

## 2.2 The flux-tube model

An ‘open’ string model of the kind described above, is essentially forced upon us if we wish to describe high- $J$  mesons within the usual valence quark picture. For glueballs, however, there is no experimental or theoretical support for a valence gluon picture. A plausible alternative is to see a

glueball as being composed of a closed loop of fundamental flux. Such a picture arises naturally in a string theory approach to gauge theories. A simple first-quantised model of glueballs as closed flux tubes was formulated some time ago [8] and has been tested with some success [9, 10] against the mass spectrum of D=2+1 SU(N) gauge theories as obtained on the lattice [5].

In this model the essential component is a circular closed string (flux tube) of radius  $\rho$ . There are phonon-like excitations of this closed string which move around it clockwise or anticlockwise and contribute to both its energy and its angular momentum. The system is (first) quantised so that we can calculate, from a Schrödinger-like wave equation, the amplitude for finding a loop of a particular radius. The phonon excitations are regarded as ‘fast’ so that they contribute to the potential energy term of the equation and the phonon occupation number is a quantum number labelling the wave-function. If we are interested in the lowest mass at a given  $J$ , as we are for the leading trajectory, then we want the potential energy [10] that corresponds to the minimum number of phonons needed to provide that  $J$

$$E(\rho) = 2\pi\rho\sigma_f + \frac{J - c}{\rho} \quad (4)$$

and we minimise this expression with respect to  $\rho$  (in much the same way as in bag models) to obtain the glueball mass  $M$

$$M = \min_{\rho} E(\rho) = (8\pi\sigma_f J)^{\frac{1}{2}}. \quad (5)$$

This corresponds to a linear Regge trajectory

$$J = \frac{M^2}{8\pi\sigma_f} \quad (6)$$

with a slope  $\alpha'_{FT} = \frac{1}{8\pi\sigma_f} = \frac{1}{4}\alpha'_R \simeq 0.22 \text{ GeV}^{-2}$ , if we input the usual value for the Regge slope (as in Section 2.1). This is similar to, but somewhat smaller than, the observed Pomeron slope. This analysis can be readily transformed into a variational calculation that minimises the Hamiltonian, without changing the final conclusion (for large enough values of  $J$ ).

The above calculation was carried out for the  $D = 2 + 1$  version of the model. In  $D = 3 + 1$  there are extra phonons corresponding to fluctuations of the loop that are orthogonal to the plane of the loop, and in addition the system can acquire angular momentum through spinning about its axis. This alters the details of the calculation, but not the qualitative conclusion.

Finally we remark that for  $SU(N > 3)$  gauge theories the fundamental string is no longer the only one that is absolutely stable, and closed loops of these higher representation strings provide an equally good model for glueballs [10, 7]. These extra glueballs will however be heavier and, to the extent that we are only interested in the leading Regge trajectory, will not be relevant for the discussion of this paper.

### 3 High-energy scattering in (2+1) dimensions

We begin by describing how the familiar Regge theory of 3 spatial dimensions can be taken over to 2 space dimensions. We confine ourselves to a brief summary here, leaving details to the Appendix.

The Pomeron has been the focus of a large number of field theoretic studies, many motivated by the ‘hard Pomeron’ and low- $x$  physics in deep inelastic scattering. Just as we asked how glueball models change when we go from 3+1 to 2+1 dimensions, it is interesting to know the predictions of these perturbative approaches when we change dimension. That will be the focus of the remainder of this Section.

### 3.1 Regge theory predictions

The optical theorem relates the total cross section to the dimensionless scattering amplitude  $T(s, t)$  by

$$\sigma_{tot} = \frac{1}{\sqrt{s}} \text{Im } T(s, t = 0). \quad (7)$$

(In two space dimensions the ‘cross section’ has dimensions of length.) As is shown in appendix A, it is given by the following contributions:

$$T(s, t) = a_0(s) + \text{background integral} + \sum \left[ \text{Regge pole contributions} \propto \left( s^{\alpha(t)} \right) \right], \quad (8)$$

where  $\alpha(t)$  describes the Regge trajectory in the Chew-Frautschi plot. This equality is based on the analytic continuation of the partial waves in  $\lambda$ , the angular momentum, and on crossing symmetry. There are two differences with respect to the 3+1 dimensional case: the background integral gives a constant contribution to the amplitude, rather than decreasing as  $\frac{1}{\sqrt{s}}$ ; and the s-wave exchange is not included in the Sommerfeld-Watson transform. In potential scattering, and even more general situations, it can be shown to be a branch point in the complex  $\lambda$  plane at threshold (see [22] and appendix B).

### 3.2 QCD<sub>2</sub> at high energies

We first give the simplest estimates of the color-singlet exchange for high energy scattering. We then comment on the failure of gluon reggeisation and review the results of Li and Tan [23] for color-singlet exchange obtained in the leading logarithm approximation. In order to develop some intuition for 2+1 dimensional physics, we finish with a discussion of the momentum dependence of hadronic structure functions.

#### 3.2.1 Color singlet exchange in leading order

If we compute the color-singlet part of a two-gluon exchange diagram between two ‘quarks’ in 2+1 dimensions (the first perturbative Pomeron model due to F. Low in 1975 [24]), we find

$$A_1^{(1)} = i\alpha_s^2 s \frac{N_c^2 - 1}{N_c^2} \int \frac{dk}{k^2(k-q)^2}, \quad (9)$$

implying, by use of the optical theorem in 2+1 dimensions (appendix A),

$$\sigma_{tot}(qq \rightarrow qq) = \alpha_s^2 \frac{N_c^2 - 1}{N_c^2} \int \frac{dk}{k^4} \quad (10)$$

The result is completely similar to the 3+1 case, except that the IR divergence is worse by one power –  $\sigma_{tot}$  has units of length. The Pomeron exchange amplitude is finite once impact factors are introduced for the hadrons – giving the incoming quarks a slight offshellness and effectively introducing a cutoff in the integral on the right-hand side of (10).

Another approach consists in computing dipole-dipole scattering (for an introduction, see [25] and references therein). Proceeding as in the 3+1 dimensional case, the leading order (large  $N$ ) dipole-dipole cross-section reads

$$\sigma_{dd} = 4\alpha_s^2 \int_{-\infty}^{\infty} \frac{d\ell}{\ell^4} (1 - \cos \ell x_{01})(1 - \cos \ell x'_{01}) = \pi\alpha_s^2 x_{<}^3 \left(3\frac{x_{>}}{x_{<}} - 1\right) \quad (2+1) \quad (11)$$

as compared to [25]

$$\sigma_{dd} = 2\pi\alpha_s^2 x_{<}^2 \left(1 + \log \frac{x_{>}}{x_{<}}\right) \quad (3+1) \quad (12)$$

where  $x_{>}$  ( $x_{<}$ ) is the greater (lesser) of the two dipole sizes  $x_{01}$  and  $x'_{01}$ . In both cases, we find a constant cross-section.

To go beyond the leading contribution, several calculational schemes are available. In particular, the BFKL Pomeron is obtained by keeping, order by order in  $g^2$ , only the leading logarithmic contribution in the perturbative expansion. The first step in calculating the amplitude for Pomeron exchange is to establish gluon reggeisation.

### 3.2.2 The issue of gluon reggeisation

In the Regge limit  $s \gg t \gg g^4$ , where  $s, t$  are the Mandelstam variables, the usual expansion in  $g^2 \log s$  yields the 0, 1 and 2-loop amplitudes for color octet exchange:

$$A_0^{(8)} = 8\pi\alpha_s G_0^{(8)} \frac{s}{t} \quad (13)$$

$$A_1^{(8)} = A_0^{(8)} \epsilon_G(t) \log \frac{s}{k^2} \quad (14)$$

$$A_2^{(8)} = \frac{1}{2} A_0^{(8)} \left( \epsilon_G(t) \log \frac{s}{k^2} \right)^2 \quad (15)$$

where  $k^2 = O(t)$  and

$$\alpha_s = \frac{g^2}{4\pi}, \quad G_0^{(8)} = \tau_{ij}^a \tau_{kl}^a, \quad \epsilon_G(t) = N_c \alpha_s \int_{-\infty}^{+\infty} \frac{dk}{2\pi} \frac{t}{k^2(k-q)^2} \leq 0 \quad (t = -q^2) \quad (16)$$

Thus, at least formally, the gluon reggeises [26]:

$$A^{(8)} = A_0^{(8)} \left( \frac{s}{k^2} \right)^{\epsilon_G(t)} \quad (17)$$

The infrared divergence in the quantity  $\epsilon_G(t)$  is linear (as opposed to logarithmic in 3+1 dimensions), and it must be so since  $\alpha_s$  carries dimension of mass. The IR “gluon mass” cutoff  $M$  has to be introduced, in which case  $\epsilon_G(t) = \frac{N_c \alpha_s}{M}$ . Physically  $M$  can be interpreted as a non-perturbative



mass that the gluon acquires at the confining scale; therefore we expect  $g^2/M = \mathcal{O}(1)$ . This however shows that, due to the infrared divergence, the result of the perturbative calculation has a linear sensitivity to physics at the confinement scale  $g^2$ , where the perturbative expansion breaks down.

In the Verlinde approach [27] to high-energy scattering adopted by Li and Tan [23], gluon reggeisation fails. However, as the authors remark, this is not necessarily in contradiction with conventional perturbative calculations, since the really physical quantity is the color-singlet exchange.

### 3.2.3 The 2+1 perturbative Pomeron

The BFKL equation was solved exactly in the presence of a gluon mass in [26]. However when this mass is taken to zero, the IR divergence shows up in the fact that the BFKL exponent  $\omega_0$  runs as  $\sim \alpha_s/M$ ; this fact could be guessed on dimensional grounds. Within perturbation theory, such a mass  $M$  can only appear as an IR regulator. The situation is in radical contrast to the 3+1 dimensional case, where the cancellation of IR divergences in the BFKL equation makes it self-consistent. In the detailed calculation, the simple structure of the infinite series is spoiled in the  $M \rightarrow 0$  limit by the re-emergence of a power dependence on  $s$  at each order due to the IR divergences. Thus, in this framework, a power-like dependence of the cross-section on  $s$  in the limit of zero gluon mass is not possible in 2+1 dimensions.

A thorough investigation of  $QCD_2$  high energy scattering was undertaken by Li and Tan [23]. In their first paper, they used the Verlinde approach [27] to obtain a one-dimensional action, where they are able to compute the (finite) color-singlet exchange exactly. They predict a

$$\sigma \propto 1/\log s \tag{18}$$

dependence of the total cross section on the center-of-mass energy. In a second publication, they re-derive this result using the dipole picture ([25] and references therein) of high-energy scattering. In this case all quantities are naturally IR-safe.

### 3.2.4 Deep inelastic scattering in 2+1 dimensions

A standard prediction of the BFKL Pomeron in 3+1 dimensions is the strong rise of the deep inelastic structure functions at low  $x$  when  $Q^2$  is large (for an introduction, see [2]):

$$F(x, Q^2) \sim \frac{x^{-\omega_0}}{\sqrt{\log 1/x}} \tag{19}$$

where  $\omega_0 = 4\frac{N_c}{\pi}\alpha_s \log 2$  is the BFKL exponent.

On the other hand, the DGLAP equation for the evolution of the moments  $M(n, Q^2)$  of the parton distributions leads to the behaviour

$$M(n, Q^2) = C_n \left( \log \frac{Q^2}{\Lambda^2} \right)^{-A_n} \tag{20}$$

where the pure number  $A_n$  is an “anomalous dimension” computed in perturbative QCD. The  $Q^2$  dependence comes from the running of the coupling  $\alpha_s$ ; in 2+1 dimensions, the equation is therefore replaced by

$$\frac{\partial M(n, Q^2)}{\partial \log Q^2} = A_n \frac{\alpha_s}{Q} M(n, Q^2) \quad (21)$$

yielding the following large  $Q^2$  behaviour:

$$M(n, Q^2) = M(n, \infty) \exp\left(-\frac{2A_n\alpha_s}{Q}\right) \simeq M(n, \infty) - 2A_n \frac{\alpha_s}{Q}. \quad (22)$$

That is to say, the structure functions tend to finite constants at large  $Q^2$ . The physical reason for this is that at large energy scales, the theory becomes free very rapidly (the effective coupling scales as  $1/E$ ), which does not allow for an evolution of the structure functions. Thus above the confinement scale, we qualitatively expect a rapid evolution in  $Q^2$  of the structure function toward its asymptotic value. Once a high  $Q^2$  has been reached, the virtual photon  $\gamma^*$  does not “see” more partons when its resolution is increased, because the amplitude that they be emitted is suppressed by  $\alpha_s/Q$ .

## 4 The D=2+1 SU(2) glueball spectrum

In the first part of this Section we discuss the technical aspects of the lattice calculation. In the second part we present the results of our calculations.

### 4.1 Technical aspects

The identification of the continuum spin of a lattice state requires novel techniques, as does the accurate calculation of the mass of a heavy, high-spin state, and we discuss these below. First however we briefly summarise the more standard aspects of the calculation.

#### 4.1.1 Masses from lattice simulations

To obtain masses we calculate Euclidean correlation functions of some well-chosen operators  $\phi_i$

$$C_{ii}(t) \equiv \langle \phi_i^\dagger(t) \phi_i(0) \rangle = \langle \phi_i^\dagger e^{-Ht} \phi_i \rangle = \sum_n |a_n|^2 e^{-E_n t}. \quad (23)$$

Here the  $E_n$  are the energies and  $a_n = \langle n | \phi_i | vac \rangle$ . If the vacuum has trivial quantum numbers, then only states with the quantum numbers of  $\phi_i$  will have  $a_n \neq 0$ . Suppose we have  $i = 1, \dots, n_0$  operators of the same quantum numbers and we also calculate the off-diagonal correlators  $C_{ij}(t)$ . Then an effective way to calculate the lightest few states with these quantum numbers is to perform a variational calculation using the basis  $\{\phi_i; i = 1, \dots, n_0\}$ . For a recent exposition of this standard method see [5].

To calculate such Euclidean correlation functions we use lattice Monte Carlo methods. As usual one needs to ensure that the operators are smooth and extended, so that they have a good projection onto the lighter physical states, and we use an iterative smearing technique for that

purpose [28]. We use an increasing number of smearing iterations (and also increase the smearing weights) as we approach the continuum. All our calculations use the standard Wilson action. The update is a 1:3 mixture of heat-bath [29, 30] and over-relaxation [31] sweeps. Because we calculate the values of many operators, the ‘measurement’ is time-consuming and we can do a significant number of these compound sweeps between measurements without significantly increasing the total cost of the calculation. We typically perform  $\mathcal{O}(10^5)$  sweeps and collect the data in  $\sim 100$  bins. Errors are estimated with a standard jackknife analysis.

#### 4.1.2 Continuum spin on a cubic lattice

Consider the eigenstates of the transfer matrix of the lattice field theory. These will belong to the irreducible representations of the cubic rotation group and will not, in general, possess the rotational properties that characterise a continuum state of a definite spin. However as  $a \rightarrow 0$  each of these states will tend to an energy eigenstate of the continuum theory that possesses some definite spin  $J$ . By continuity for sufficiently small  $a$  the rotational properties of this lattice state will be arbitrarily close to those of a continuum state of spin  $J$ . We will therefore refer to such a state not only by its lattice representation but also by the appropriate continuum spin  $J$ . To be able to do this we need to identify, for each such lattice state, what continuum  $J$  it tends to as  $a \rightarrow 0$ . Once we know this then we can perform a standard continuum extrapolation of the calculated lattice masses so as to obtain the continuum mass of the spin  $J$  glueball.

A detailed investigation into how to do this was presented in [6]. Here we shall apply a systematic version of the method that was presented there under the name ‘Strategy II’. We briefly remind the reader of this method.

The operators we use lie in definite lattice irreducible representations (IRs), and we use the variational method [32] to extract estimates for the eigenstates (in our operator basis) and their masses. In this way we calculate the mass of the lightest state and of several excited states in the given lattice IR – typically the number is one third of the number of operators we are using. To identify which  $J$  each of these states tends to, we do a simple Fourier analysis of the wave function of the corresponding diagonalised operator. To do this we measure the correlations between it and a ‘probe’ operator that we are able to rotate to a good approximation by angles smaller than  $\frac{\pi}{2}$ . This provides a measurement of the wave function. We check the rotational properties of the probe by measuring the vacuum wave function; typically it is found to be isotropic at the one percent level, which is taken as evidence that the probe has good rotational properties. We are mainly interested in the dominant component and the fact that there is an uncontrolled uncertainty of a few percent in the measurement of the wave function does not impede significantly the procedure of determining the spin of a state in the continuum limit. This is so because one is usually discriminating between a constant and a change of sign behaviour of the wave function. In principle, the continuum extrapolation of these coefficients should determine uniquely the spin of the glueball. In practice, it usually turns out that there is already a very dominant coefficient at finite lattice spacing – except when a crossing of states occurs – as we shall see in an example later on.

### 4.1.3 The multi-level algorithm

A state with high spin will generically have a large mass, and the value of the corresponding correlation function can be very small. Indeed, even if we have a perfect operator the value of the correlator will be  $O(e^{-aM_J n_t})$  at  $t = an_t$  and if  $aM_J \gg 1$  then it will be in danger of being swamped by the statistical errors. In practice it is not possible to restrict oneself to values of  $a$  such that  $aM_J \ll 1$  for all values of  $J$  that are of interest. Especially so because we need a range of  $a$  that is large enough for a well-controlled continuum extrapolation.

To deal with this problem we make use of a recently proposed error reduction algorithm for glueball correlators [15]. It proved very useful on all but the smallest lattice spacings (i.e. on  $\beta = 6, 7.2, 9, 12$ ). For  $6 \leq \beta \leq 9$ , we used  $\mathcal{O}(500)$  sub-sweeps, while we decreased their number to 50 at  $\beta = 12$ . These sub-sweeps are done on sub-lattices which represent “time-blocks” of width 4. Our experience is that it is more efficient to do all these sweeps at one fixed time-block (that is, a 2-level algorithm) rather than splitting up the sweeps between width 2 and width 4 blocks (that is, a 3-level algorithm). This was noted previously in [16], where a multi-level algorithm was applied to Polyakov loop measurements, and suggested in [33].

The choice of the number of sweeps was done on the basis of the thumb-rule  $n_{sweeps} = e^{m\Delta t}$ , where in our case  $\Delta t = 4a$  and the algorithm was optimised for the spin 4 glueball, that is  $m = m_4$ . Indeed when one is measuring large portions of the spectrum, a compromise has to be made. For the lighter states, it is more efficient to do few sub-sweeps, while the heavier states require more of them. That is, for the same computer time, we could have measured the lightest glueball mass more accurately had we not used a 2-level algorithm, but we would then have far less accurate and reliable results for the spin 4 and 6 glueballs – the main goal of the present simulations.

The multi-level algorithm enables us to apply the variational method on the correlation matrices at 2 and 3 lattice spacings even on the coarsest lattice. Very often, when the correlators are measured in the traditional way, the noise that dominates the signal of the heavier states spoils the positivity of the correlation matrices if the method is not applied between 0 and 1 lattice spacing, thus impeding the variational calculation. In our case however the very massive eigenstates benefit most from the sub-averaging procedure and the positivity is maintained. Usually the orthogonalised operators have reached their mass plateaux (within error bars) by three lattice spacings for the data we present in this paper; this increases our confidence in the reliability of the variational method.

At  $\beta = 18$ , the correlation length  $1/\sigma \simeq 12a$ ; that would be the natural width in the Euclidean time direction over which to do sub-sweeps. However that would mean extracting the masses at time separations of that order. It turns out that our smeared operators have sufficiently good overlaps onto the physical states to reach a plateau far earlier than 12 lattice spacings. For that reason, we did not apply the multi-level algorithm to that case. Nevertheless we regard this as a consequence of the improved smoothness of the operators close to the continuum rather than as a defect of the multi-level algorithm.

## 4.2 Results

In Table 1 we list the values of the masses we calculate on  $L^3$  lattices at various values of  $\beta = 4/ag^2$ . The masses are in lattice units and are labelled both by the lattice IR to which they belong, and by the spin  $J$  of the state to which they tend in the continuum limit. The latter assignment is

achieved as described above, and an explicit example will be given below. We also have calculated the confining string tensions as indicated. The string tension provides a natural dynamical length scale  $\xi \equiv 1/\sqrt{\sigma}$  which tells us how small the lattice spacing  $a$  is,  $a/\xi = a\sqrt{\sigma}$ , and how large our lattice size,  $aL$ , is,  $aL/\xi = aL\sqrt{\sigma}$ .

Since high- $J$  states are expected to be very extended, it is important to check that our  $J = 0, 2, 4, 6$  mass estimates are not subject to large volume corrections. This is the first thing we do in this subsection. We then give an explicit example of the Fourier coefficients which we use to identify the  $J$  of the state. Finally we discuss the extrapolation to the continuum limit.

#### 4.2.1 Finite volume effects

As one can see from Table 1, the spatial size that we use for most of our calculations satisfies  $aL\sqrt{\sigma} \sim 4$ . This choice was based on earlier finite volume studies [5] that showed that it appeared to be large enough for the lightest glueball states. In particular, on such a volume the lightest state of two periodic flux loops (which can couple to local glueball operators) will be heavier than the lightest few  $A_1$  states and the lightest  $A_3$  state. In this paper, however, we are interested in higher spin states that may be significantly more extended than these lightest states, so it is important to check for finite volume corrections by performing at some  $\beta$  the same calculations on much larger volumes. We do this at  $\beta = 7.2$ , where the spatial extent of our comparison volume is twice as large. In addition we perform a more limited comparison at a finer lattice spacing,  $\beta = 12$ , on a comparison lattice that is about 30% larger.

We see from Table 1 that there is in fact no significant change in any of the masses listed when we double the lattice size from  $aL\sqrt{\sigma} \sim 4$  to  $aL\sqrt{\sigma} \sim 8$  at  $\beta = 7.2$ . In particular this is true for the  $J = 4$  and  $J = 6$  states where our concern is greatest. We note also that on the  $L = 40$  lattice a state composed of two periodic flux loops will have a mass  $am_T \sim 2La^2\sigma \simeq 3.45$  which is much heavier than any of the masses listed and so it will not be a source of finite volume corrections there. From the comparison we infer that these ‘torelon’ states cause no problem on the  $L = 20$  lattice even though their mass  $am_T \sim 1.7$  is light enough for it to mix with the states of interest. This tells us that in general such mixing will not be important even where it is possible. This is consistent with the observation [5] that in many respects  $SU(2)$  is close to  $SU(\infty)$ , since in the latter case the mixing will vanish.

The more limited finite volume check at  $\beta = 12$  also shows no significant volume variations for the  $J = 4$  and  $J = 6$  states, as well as the  $J = 0$  states. On the other hand there are some anomalies in the  $J = 2$  part of the  $A_3$  spectrum. Since on these two lattices the ‘torelon’ state has a mass  $am_T \sim 0.9$  and  $am_T \sim 1.2$  respectively it is possible that it is mixing with some nearly degenerate  $A_3$  glueball states on both the lattice sizes, and that this explains the anomalies. However we also remark that these calculations were performed at an early stage (unlike those at  $\beta = 7.2$ ) and a different basis of operators was used on the two volumes. Thus it is not clear how seriously we should take the discrepancies observed in the  $A_3$  sector.

### 4.2.2 The Fourier coefficients

As described in Section 4.1.2, we determine the ‘ $J$ ’ of a lattice energy eigenstate by a Fourier decomposition of its wavefunction. For example for a state in the trivial  $A_1$  lattice IR we have

$$|\psi_1\rangle = \sum_{n \geq 0} c_n |(j = 4n)^+\rangle|_{lat} \quad \text{with} \quad \sum_n |c_n|^2 = 1. \quad (24)$$

The Fourier decomposition is performed using as a probe a loop  $\mathcal{O}$  for which we have a number of other loops  $\mathcal{O}_\theta$  that are (to a good approximation) copies of  $\mathcal{O}$  rotated by angles  $\theta$  that are not multiples of  $\pi/2$ :

$$\langle vac | \mathcal{O}_\theta | \psi_1 \rangle = \sum_{n \geq 0} c_{\mathcal{O}} c_n e^{i4n\theta} \quad (25)$$

(where  $c_{\mathcal{O}}$  is independent of  $n$  in the limit where  $\mathcal{O}_\theta$  is an exact rotated copy of  $\mathcal{O}$ ). Note that since the angular resolution is  $O(a)$  one can attempt to resolve spins up to  $J_{max} \sim O(1/a)$  in this way. In Table 2 we show the Fourier coefficients calculated at the lattice spacings  $\beta = 7.2, 9, 12, 18$ . The table shows the normalised  $|c|^2$  coefficients corresponding to the spin that the state is assigned in the continuum limit. We see that the states that become  $0^+$  have very isotropic wavefunctions even at the finite lattice spacings considered. The spin 4 coefficients of the spin-4-to-be states vary a lot more. Let us look at the fundamental spin 4 glueball in more detail.

The coefficient is very close to one at  $\beta = 7.2, 9$  and  $18$ , but shows a big dip at  $\beta = 12$ . We attribute this to the crossing of the lightest spin 4 state and the  $0^{+***}$ . Indeed looking at the masses in table 1, we observe that these two states are always nearly degenerate, the spin 4 being slightly heavier on the coarse lattices and slightly lighter on the finer lattices, while they are closest precisely at  $\beta = 12$ . As was pointed out in [6], an ‘accidental’ degeneracy like this automatically leads to maximal quantum mechanical mixing between the states, since there is no lattice symmetry to prevent that. Taking this into account, the observed evolution of the Fourier coefficient is not implausible.

At  $\beta = 6$  we did not perform a Fourier decomposition but rather chose the value of  $J$  using the level ordering already established for the other values of  $\beta$ . The reason we did not perform such a decomposition is that this calculation was originally intended as a test of the multi-level algorithm rather than as a contribution to the present study. However given its accuracy it seemed wasteful not to use it. We have a less accurate older study [6] where the Fourier decomposition was performed and that supports our spin identification. In addition the mass of the identified  $4^-$  state, and the fact that it should be (nearly) degenerate with the  $4^+$  leaves no doubt about the correctness of the  $J = 4$  identification in this case as well.

### 4.2.3 Continuum extrapolation

Our continuum extrapolation of the states in the  $A_1$  and  $A_3$  representations is entirely conventional and follows [5, 6]. We plot the glueball masses in units of the string tension as a function of  $\sigma a^2$ , and attempt a linear fit

$$\frac{am_G(a)}{a\sqrt{\sigma(a)}} \equiv \frac{m_G(a)}{\sqrt{\sigma(a)}} = \frac{m_G(0)}{\sqrt{\sigma(0)}} + ca^2\sigma. \quad (26)$$

This is motivated by the fact that we know the leading lattice correction to be  $O(a^2)$  for the plaquette action. If such a fit has a bad confidence level, then we remove the coarser lattice data until a good fit is obtained. We require that at least three points are left.

Fig. 1 shows the actual extrapolation for the lightest state of each spin. We observe as in [6] that the evolution is weak. Note also that thanks to the error reduction technique employed, the error bars corresponding to the coarser lattices do not appear very much larger than those associated with finer lattices. Table 3 gives the continuum spectrum in units of the string tension, as well as the confidence level and the number of different lattice spacings included in the fit. For the fundamental states of spin 0, 2, 4 and 6, the confidence levels are good and include all five lattice spacings.

Not surprisingly, the second and third excited states have less reliable extrapolations. A slight dependence of the masses obtained for the excited states on the basis used in the variational method is likely to be the cause of the stronger spread of the lattice data in the extrapolation plot. Notice for instance that all four states shown on Fig. 1 appear slightly lighter at  $\beta = 18$  than at the other lattice spacings.

## 5 $SU(N > 2)$

As we remarked in Section 1, it is only in the  $N \rightarrow \infty$  limit, where all glueballs become stable, that one can hope to identify the ideal linear Regge trajectory. In principle all one needs to do is to repeat the above  $SU(2)$  calculation for  $N = 3, 4, 5, \dots$ . We know from [5] that the approach to  $N = \infty$  is rapid so that the first few values of  $N$  should suffice for a good extrapolation to all values of  $N$ . However while such a calculation is certainly feasible, it is beyond the very limited computational resources currently available to us. Fortunately we are able to finesse this practical problem using the fact that it has been shown in [6] that the lightest state in the lattice  $A_2$  IR, which contains  $J^P = 0^{-+}, 4^{-+}, 8^{-+}$ , is in fact the  $4^{-+}$  rather than the  $0^{-+}$ . This confirmed earlier suggestions, based on an analysis of the predictions of flux tube models [10], that the lightest  $0^{-+}$  should be much more massive than the lightest observed  $A_2$  state, while the latter was consistent with the model prediction for the lightest  $4^{-+}$  state. Due to parity doubling in  $D = 2 + 1$  this mass is the same as that of the  $4^{++}$  (in the infinite volume continuum limit). Thus we can use the lightest states in the  $A_1, A_3$  and  $A_2$  lattice representations, as calculated for various  $SU(N)$  groups in [5], to provide us with the lightest  $J = 0, 2, 4$  glueball masses. (Note that this means that the masses labelled in the tables of [5] as being those of the lightest  $0^{-+}$  should in fact be relabelled as being the lightest  $4^{-+}$ .) This is more limited than our explicit  $SU(2)$  calculation where we also identify the  $J = 6$  glueball, but it is adequate given the presumption that there will be no qualitative change as we increase  $N$  from  $N = 2$ .

The assumption that for  $SU(N > 2)$  the lightest  $A_2$  state is the  $4^{-+}$  is very reasonable given that this is so in  $SU(2)$  [6] and that it is predicted to be so by generic flux loop models [10]. Nonetheless it is an assumption and should be checked. We have therefore performed such a check in the  $SU(5)$  case, at  $\beta = 64, L = 24$ , where  $\sigma^{-1/2} \simeq 6a$ . Using a 16-fold rotated triangular probe operator reveals that the wave function of our best  $A_2$  operator, measured at a Euclidean time separation of one lattice spacing, behaves like  $\sin 4x$ , with a normalised coefficient consistent with 1 at the few percent level. This confirms the correctness of our assumption.

## 6 Physical discussion

We begin by asking what our glueball spectrum tells us about the nature of the leading glueball Regge trajectory, both for  $SU(2)$  and for larger  $N$ . We then compare what we find to the predictions of the simple glueball models in Section 2. Finally we discuss what role this trajectory will play in high energy scattering.

### 6.1 The glueball spectrum in a Chew-Frautschi plot

In Fig. 2 we plot our continuum  $SU(2)$  glueball spectrum in a Chew-Frautschi plot of  $m^2/\sigma$  against the spin  $J$ . We see that the lightest  $J = 0, 2, 4, 6$  masses appear to lie on a straight line. If we fit them with a linear function  $J = \alpha(t)$ , where  $\alpha(t) = \alpha_0 + \alpha't$  and  $t = m^2$ , then we obtain

$$2\pi\sigma\alpha'_{(m)} = 0.322(16) \quad \alpha_0^{(m)} = -1.18(11) \quad (27)$$

with a confidence level of 65%. (If we drop the  $J = 0$  state from the fit, the errors become somewhat larger, but the trajectory is essentially the same.) Thus we reach the remarkable conclusion that the lightest glueballs of spin  $J$  fall on a linear Regge trajectory. This is the leading trajectory, hence the index ( $m$ ) standing for ‘mother trajectory’.

Although there is more uncertainty in establishing the excited spectrum, particularly in the spin 2 sector where finite volume effects are not completely understood, we also fit the  $0^{+*}$ ,  $2^{**}$  and  $4^*$  states to a straight line and find

$$2\pi\sigma\alpha'_{(d)} = 0.265(36) \quad \alpha_0^{(d)} = -2.20(44) \quad (28)$$

with a confidence level of 93%. This ‘daughter’ trajectory is approximately parallel to the leading one, and its intercept is down by about one unit.

As we explained in Section 5, we can also say something about the leading Regge trajectory in  $SU(N > 2)$  gauge theories, if we use the masses calculated in [5] and relabel as  $4^{-+}$  the state that is labelled there as the lightest  $0^{-+}$ . Since the  $4^{-+}$  and  $4^{++}$  are degenerate in the (infinite volume) continuum limit, this gives us the  $0^{++}$ ,  $2^{++}$  and  $4^{++}$  continuum masses for  $N = 2, 3, 4, 5$ . A linear fit,  $J = \alpha(m^2) = \alpha_0 + \alpha'm^2$ , works in all cases and yields:

[5] data	$2\pi\sigma\alpha'_{(m)}$	$\alpha_0^{(m)}$	conf. lev.
$N = 2$	0.324(15)	-1.150(75)	89%
$N = 3$	0.384(16)	-1.144(71)	54%
$N = 4$	0.374(18)	-1.068(75)	71%
$N = 5$	0.372(22)	-1.036(88)	86%

We have also included the result for  $SU(2)$  and we note that the parameters of the trajectory are in very good agreement with the data of this paper. It is clear that for all the number of colors available, the linear fit has a very good confidence level.

We conclude that all  $SU(N)$  gauge theories possess approximately linear Regge trajectories, with slopes 0.3–0.4 in units of  $2\pi\sigma$ , and intercepts close to -1, which appear to be approaching that value as  $N \rightarrow \infty$ .



## 6.2 Comparison to glueball models

As we saw in Section 2, the closed flux tube model of glueballs predicts a leading Regge trajectory that is linear, with a slope that is independent of  $N$ :

$$2\pi\sigma \alpha'_{FT} = \frac{1}{4} \quad \forall N \quad (29)$$

The adjoint string model also predicts a linear Regge trajectory but with a slope  $2\pi\sigma_a \alpha'_{AS} = 1$  that in general depends on  $N$  through the  $N$  dependence of  $\sigma_a/\sigma$ . Lattice calculations [21] (and some theoretical arguments [34]) support a dependence that is close to Casimir scaling,

$$\frac{\sigma_a}{\sigma} = \frac{C_A}{C_F} = 2 \frac{N^2}{N^2 - 1}. \quad (30)$$

Assuming this, the slope predicted by the adjoint string model becomes

$$N = 2 : \quad 2\pi\sigma \alpha'_{AS} = \frac{3}{8} \quad (31)$$

$$N = \infty : \quad 2\pi\sigma \alpha'_{AS} = 2 \times (2\pi\sigma \alpha'_{FT}) = \frac{1}{2} \quad (32)$$

Interestingly, for all the  $N$  considered, the lattice result for  $\alpha'$  is almost exactly at the midpoint between the two model predictions. We illustrate this fact in Fig. 3. We might speculate that even if both models are valid, thus producing two glueball trajectories with different slopes, at finite  $N$  mixing will deform these trajectories from exact linearity and that such a deformation will be greatest at some lower  $J$  where the states of the two trajectories are closest and also where we perform our calculations.

We observe that the intercept of the leading Regge trajectory that we have obtained is close to -1, and becomes perhaps even closer at larger  $N$ , as we see if we plot

$$\Delta \equiv -(\alpha_0 + 1), \quad (33)$$

in Fig. 4. Now we recall that in D=3+1 [2] the fact that the color-singlet amplitude is, order by order, down by a factor of  $N\alpha_s$  with respect to the color octet exchange amplitude (see Section 3.2) can be interpreted as coming from an expansion of the signature suppression factor around  $J = 1$ , using the fact that in this picture  $\alpha(t = 0) = 1 + O(\alpha_s)$ . A similar argument will work in D=2+1 as long as  $\alpha(t = 0)$  is near an odd integer. We assume that  $\alpha(t = 0) \simeq 1$  is disfavoured since it would lead to a rapidly rising cross-section, and so the next possibility would be  $\alpha(t = 0) \simeq -1$ , as observed in our calculations. This line of reasoning relies on the idea that the perturbative calculation remains qualitatively valid even as  $t \rightarrow 0$ , which is of course not guaranteed.

At finite  $N$  Regge trajectories are not expected to rise linearly at arbitrarily large  $t = m^2$ . In particular we should expect that due to mixing between high spin glueballs and multi-glueball scattering states, for which

$$\alpha(t) \propto \sqrt{t}, \quad (34)$$

the local slope of the trajectory decreases as  $J$  increases. This effect is, however, suppressed by  $\frac{1}{N^2}$  in the large  $N$  limit.

### 6.3 High-energy scattering prediction

The contribution of the leading glueball trajectory to the total cross-section behaves as

$$\Delta\sigma \propto s^{\alpha_0 - \frac{1}{2}}, \quad (35)$$

which means, given our calculated value  $\alpha_0 \simeq -1$ , that it is suppressed as  $\sim s^{-\frac{3}{2}}$ . Thus the high energy scattering of glueballs is not dominated by Regge pole exchange in 2+1 dimensions; at least if we believe that the cross section should be constant at high energies (up to powers of  $\log s$ ).

Going back to section 3.1, we note that the other terms contributing to the scattering amplitude are the isolated s-wave amplitude  $a_0(s)$  and the background integral. Because there is a unitarity bound on each partial wave separately, namely

$$\text{Im } a_n \geq |a_n|^2, \quad (36)$$

the contribution of any partial wave amplitude to the total cross-section is bounded by  $\sim s^{-\frac{1}{2}}$ . Thus this s-wave amplitude will not dominate either at high energies. That, then, only leaves the background integral. If the partial wave amplitude  $a(\lambda, t)$  were meromorphic in the region  $0 < \text{Re } \lambda < \frac{1}{2}$ , we would simply get additional Regge pole contributions, which should show up as physical states by analytic continuation. Therefore there must be a more complicated singularity structure in that region. For instance it is well known that  $\lambda = 0$  is a logarithmic branch point of the partial wave amplitude  $a(\lambda, t)$  at low energies ([22]; see also appendix B). Also, Li and Tan [23] remark in their second publication that the dipole-dipole forward scattering amplitude can be written as a contour integral in the complex  $\lambda$  plane around  $\lambda = 0$ :

$$A(d, d', s) = \frac{2\pi g^2 d d'}{N_c} \frac{1}{\log s} = -\frac{2\pi g^2 d d'}{N_c} \int \frac{d\lambda}{2\pi i} s^\lambda \log \lambda \quad (37)$$

where  $d, d'$  are the sizes of the scattering dipoles; again, the logarithmic branch point seems to dominate the scattering process. This intriguing similarity suggests a universal contribution from the point  $\lambda = 0$ .

## 7 Conclusion

In this paper we have carried out a lattice calculation of part of the higher spin mass spectrum of  $SU(2)$  gluodynamics in 2+1 dimensions. Such a calculation can tell us what the leading glueball Regge trajectory looks like and, in particular, whether it resembles the Pomeron.

To provide some motivation for this question, we showed how simple glueball models predict linear Regge trajectories, with small slopes, in both 2+1 and 3+1 dimensions. We emphasised that, unlike the case of  $q\bar{q}$  mesons, there are two natural models: the open adjoint string that is the natural extension of the usual Regge model for mesons, and the closed flux tube which has no analogue for the usual mesons, but which arises naturally in string theory approaches to  $SU(N)$  gauge theories. One may speculate that both models contribute and that there are two Pomerons (for which there is some experimental evidence).

Another part of our motivation for a study in D=2+1 is an intuition that in high energy scattering the colliding glueballs should behave like ‘black segments’ (analogous to the ‘black discs’

of  $D=3+1$ ) so that the cross-section is approximately constant at high  $s$ . Of course in  $D=2+1$  we have no experimental support for such an intuition and we therefore investigated how various field theoretic approaches to high energy scattering can be translated from  $D=3+1$  to  $D=2+1$ . The generic change is that infrared divergences become much more severe so that, for example, one can no longer predict directly from the BFKL equation [26] a power-like dependence of the cross section in  $s$ . However there exist alternative analyses [23] done in the framework of leading-logarithmic perturbative expansion that do indeed obtain cross-sections which are constant (up to logarithms).

The framework for Regge poles is Regge theory and we saw that there are significant changes when we go from 3 to 2 spatial dimensions. In particular the  $l = 0$  partial wave is not included in the Sommerfeld-Watson transform and the background integral is only down by  $1/\sqrt{s}$ . (In  $D=2+1$  the intercept of a trajectory  $J = \alpha(t)$  that gives a constant cross section is at  $\alpha(0) = 1/2$  in contrast to  $\alpha(0) = 1$  in  $D=3+1$ .) One can imagine that the complicated singularity structure at  $Re\lambda = 0$ , which is not associated with particles of the theory, might be promoted to a dominant contribution to the high energy cross section.

With the above background in mind, we presented the results of our lattice calculation of the higher spin glueball spectrum. This is a pioneering calculation and like all such calculations can be improved upon in many respects. However we are confident in the robustness of the results that we obtain. In particular, extrapolating our masses to the continuum limit shows that the leading Regge trajectory in the  $(\text{mass})^2$  versus spin plane is in fact linear (to a good approximation). Moreover it has a small slope that lies roughly midway between the predictions of the flux tube and adjoint string models. The intercept at  $t = m^2 = 0$  is  $\alpha_0 \simeq -1$ . We identified a parallel daughter trajectory, lying about one unit of  $J$  lower. We were also able to determine the leading Regge trajectory for other  $SU(N)$  groups and found that the result depends very little on  $N$ . In particular it is essentially the same for the theoretically interesting  $SU(\infty)$  limit.

The very low intercept of the leading glueball trajectory ( $\alpha_0 \simeq -1$ ) indicates that the moving Regge pole corresponding to these glueball states gives a negligible contribution to high-energy scattering in  $2+1$  dimensions. We concluded that there must be a more complicated singularity structure of the partial wave amplitude in the complex angular momentum plane  $\lambda$ . Evidence for a possibly universal branch point at  $\lambda = 0$  comes mainly from low-energy potential scattering (where the result is independent of the potential [22]) and is suggested by the  $\frac{1}{\log s}$  scattering amplitude found by Li and Tan in  $QCD_2$  high-energy scattering.

These statements are all quite different to what one expects in  $3+1$  dimensions. There the phenomenological Pomeron is widely thought to be related to the glueball spectrum of the  $SU(3)$  gauge theory, in which case the leading glueball trajectory had better have an intercept  $\alpha_0$  around 1. We are currently performing a similar calculation in  $D=3+1$   $SU(3)$  gluodynamics. Preliminary results [35] indicate that a straight line passing through the  $2^{++}$  and  $4^{++}$  states in a Chew-Frautschi plot does not pass through the  $0^{++}$  (in contrast to what we found in  $D = 2+1$ ) and has parameters  $\alpha_0 = 1.03(40)$  and  $2\pi\sigma\alpha' = 0.27(9)$ ; the latter translating to  $\alpha' \simeq 0.22(8)\text{GeV}^2$  if we use  $\sigma \simeq (0.44\text{GeV})^2$ . These characteristics are broadly compatible with the well known properties of the soft Pomeron.

# Acknowledgements

One of us (HM) thanks the Berrow Trust for financial support. The numerical calculations were performed on PPARC and EPSRC funded workstations in Oxford Theoretical Physics.

— \* \* \* —

## A Regge theory in 2+1 dimensions

The theory of the  $S$ -matrix can be developed in an entirely analogous way to the 3+1 dimensional case, using the usual fundamental postulates [2]:

- the  $S$ -matrix is Lorentz invariant;
- the  $S$ -matrix is unitary;
- the  $S$ -matrix is an analytic function of Lorentz invariants, with only those singularities required by unitarity.

We denote by  $A$  the  $a + b \rightarrow c + d$  amplitude. In 3+1 dimensions, this is a dimensionless quantity, whereas in 2+1 dimensions, it has unit of mass. Therefore we define

$$T(s, t) = \frac{1}{\sqrt{s}} A(s, t) \quad (38)$$

The partial wave expansion in the  $s$ -channel reads

$$T(s, t) = a_0(t) + 2 \sum_{\lambda \geq 1} a_\lambda(t) C_\lambda \left(1 + \frac{2s}{t}\right). \quad (39)$$

Here

$$1 + \frac{2s}{t} = \cos \theta \quad (s - \text{channel}) \quad (40)$$

in the  $s$  channel and

$$C_\lambda(\cos \theta) = \cos \lambda \theta \quad (41)$$

is a Chebyshev polynomial. The absence of a factor 2 in the first term originates from the geometric difference between the spin 0 and the other partial waves. If we define a parity axis along the axis of the collision, then while the left- and right-winding spin  $\lambda$  wave functions add up to  $2 \cos \lambda \theta$ , in the spin 0 sector the negative parity state does not have a wave function (as is the case in 3+1 dimensions); therefore only the  $0^+$  state contributes as a partial wave. This separation of the spin 0 sector is necessary in order to carry out the analytic continuation in  $\lambda$  through the Sommerfeld-Watson transform. In 2+1 dimensions, the complications due to the signature  $\eta = \pm 1$  also appears

since the wave functions of spin  $\lambda$  are associated with a phase  $(-1)^\lambda$  under a rotation by  $\pi$ . Thus we have to introduce two analytic functions  $a^+(\lambda, t)$  and  $a^-(\lambda, t)$ , so that

$$T(s, t) = a_0(t) + i \int_C d\lambda \sum_{\eta} \frac{\eta + e^{-i\pi\lambda}}{2} \frac{a^{(\eta)}(\lambda, t)}{\sin \pi\lambda} C(\lambda, 1 + \frac{2s}{t}) \quad (42)$$

We now want to deform the contour as is done in 3+1 dimensions. However because

$$C_{\lambda}(z) \sim z^{|\lambda|} \quad (|z| \rightarrow \infty), \quad (43)$$

we cannot reduce the 'background integral' by pushing it to  $\text{Re } \lambda = -\frac{1}{2}$ . Therefore we integrate along the imaginary axis and arrive at the following expression:

$$\begin{aligned} T(s, t) = & a_0(t) + i \int_{\epsilon-i\infty}^{\epsilon+i\infty} d\lambda \sum_{\eta} \frac{\eta + e^{-i\pi\lambda}}{2} \frac{a^{(\eta)}(\lambda, t)}{\sin \pi\lambda} C(\lambda, 1 + \frac{2s}{t}) + \\ & \sum_{\eta} \sum_n \frac{\eta + e^{-i\pi\alpha_{n\eta}}}{2} \frac{2\pi \text{Res}_{n\eta}(t)}{\sin \pi\alpha_{n\eta}(t)} C(\alpha_{n\eta}(t), 1 + \frac{2s}{t}) \end{aligned} \quad (44)$$

So unless  $a_0(t)$  and the background integral vanish, we obtain

$$T(s, t) \sim s^{\max(\bar{\alpha}(t), 0)} \quad (45)$$

where  $\bar{\alpha}(t)$  is the pole with the largest real part ("leading Regge pole"). Using the optical theorem at high energies

$$\sigma_{tot} = \frac{1}{s} \text{Im } A(s, t=0) = \frac{1}{\sqrt{s}} \text{Im } T(s, t=0), \quad (46)$$

we obtain the prediction, for scattering driven by Regge-pole-exchange,

$$\sigma_{tot} \sim s^{\bar{\alpha}(0) - \frac{1}{2}} \quad (47)$$

If all Regge trajectories have negative intercept, the background term prevails at high-energy. In the case of potential scattering,  $\lambda = 0$  is an accumulation point of Regge poles when  $t \rightarrow 0$  [22]. It is for that reason that we kept the background integral along  $\text{Re } \lambda = \epsilon$ .

## B Potential scattering & bound states in the plane

The Ansatz

$$\psi(r, \varphi) = \sum_{\lambda=-\infty}^{\infty} \frac{\phi_{\lambda}(r)}{\sqrt{r}} e^{i\lambda\varphi} \quad (48)$$

plugged into the Schroedinger equation leads to the following radial equation for  $\phi_{\lambda}$ :

$$-\phi_{\lambda}(r)'' + \left( \frac{(\lambda^2 - \frac{1}{4})}{r^2} + V(r) \right) \phi_{\lambda}(r) = E\phi_{\lambda}(r) \quad (49)$$

Thus there is a trivial correspondence between scattering in 3 dimensions and 2 dimensions via the substitution:

$$\ell = \lambda - \frac{1}{2} \quad \Rightarrow \quad \ell(\ell + 1) = \lambda^2 - \frac{1}{4} \quad (50)$$

This effective shift in the angular momentum has important consequences. Regge originally showed for a large class of potentials in 3d scattering that the partial wave amplitudes are meromorphic in  $\ell$  in the region  $\text{Re } \ell > -\frac{1}{2}$ ; this corresponds to the region  $\text{Re } \lambda > 0$  in 2d. It was already known in the sixties that at threshold  $E \rightarrow 0$ , there is an accumulation of an infinite number of Regge poles around  $\lambda = 0$ .

### The point $\lambda = 0$

We momentarily restore the ordinary units of quantum mechanics. Because of the Heisenberg uncertainty principle  $p_r \geq \hbar/2r$ , we have

$$E \geq \frac{\hbar^2}{8mr^2} + \frac{\hbar^2}{2m} \frac{\lambda^2 - \frac{1}{4}}{r^2} + V, \quad (51)$$

which at  $\lambda = 0$  simply reduces to  $E \geq V(r)$ . Thus this exact cancellation between zero-point quantum fluctuations implies that any attractive potential, however weak, will create a bound state at  $\lambda = 0$ . Indeed, a heuristic calculation can be found in [36] showing that the binding energy is a non-perturbative expression in the potential:

$$E \simeq \exp -\frac{1}{\int V(r)rdr} \quad (52)$$

**Low-energy potential scattering** It was shown in [22] that under very general conditions, the  $s$ -wave amplitude vanishes logarithmically at threshold. This can be interpreted as a branch point singularity in the complex  $\lambda$  plane:

$$a_0 \sim \frac{\pi}{2 \log k} = \frac{\pi}{2} \int \frac{d\lambda}{2\pi i} k^{\lambda} \log \lambda \quad (k \rightarrow 0) \quad (53)$$

## References

- [1] A. B. Kaidalov, arXiv:hep-ph/0103011.
- [2] J.R. Forshaw, D.A. Ross, “Quantum Chromodynamics and the Pomeron”, Cambridge Lecture Notes in Physics, CUP 1997
- [3] P.V. Landshoff, arXiv:hep-ph/0108156.
- [4] G. 't Hooft, Nucl. Phys. B72 (1974) 461.  
E. Witten, Nucl. Phys. B160 (1979) 57.  
S. Coleman, 1979 Erice Lectures.  
A. Manohar, 1997 Les Houches Lectures, hep-ph/9802419.
- [5] M. J. Teper, Phys. Rev. D **59** (1999) 014512 [arXiv:hep-lat/9804008].
- [6] H. B. Meyer and M. J. Teper, Nucl. Phys. B **658** (2003) 113 [arXiv:hep-lat/0212026].
- [7] B. Lucini and M. Teper, Phys. Rev. D64 (2001) 105019 [arXiv:hep-lat/0107007].
- [8] N. Isgur and J. Paton, Phys. Rev. D **31** (1985) 2910.
- [9] T. Moretto and M. Teper, arXiv:hep-lat/9312035.
- [10] R. W. Johnson and M. J. Teper, Phys. Rev. D **66** (2002) 036006 [arXiv:hep-ph/0012287].
- [11] S. Dalley and B. van de Sande, Phys. Rev. D63 (2001) 076004 [arXiv:hep-lat/0010082].
- [12] J. Maldacena, Adv. Theor. Math. Phys. 2, 231 (1998) [Int. J. Theor. Phys. 38, 1113 (1998)][hep-th/9711200]
- [13] E. Witten, Adv. Theor. Math. Phys. 2, 505 (1998) [hep-th/9803131]
- [14] Csaba Csaki, Hiroshi Ooguri, Yaron Oz, John Terning, JHEP 9901:017,1999 [hep-th/9806021];  
N.R. Constable, R.C. Myer, JHEP 9910:037,1999, [hep-th/9908175]; R.C. Brower, S.D. Mathur, C-I Tan, Nucl. Phys. B587:249-276, 2000 [hep-th/0003115]
- [15] H. B. Meyer, JHEP **0301** (2003) 048 [arXiv:hep-lat/0209145].
- [16] M. Luscher and P. Weisz, JHEP **0207** (2002) 049 [arXiv:hep-lat/0207003].
- [17] D. Perkins, *Introduction to High Energy Physics* (Addison-Wesley, 1972)
- [18] B. Lucini and M. Teper, JHEP 0106 (2001) 050 [arXiv:hep-lat/0103027].
- [19] B. Lucini, M. Teper and U. Wenger, Phys.Lett. B545 (2002) 197 [arXiv:hep-lat/0206029].
- [20] L. Del Debbio, H. Panagopoulos and E. Vicari, JHEP 0208 (2002) 044 [arXiv:hep-th/0204125].
- [21] S. Deldar, Phys. Rev. D62 (2000) 034509 (hep-lat/9911008).  
G. Bali, Phys. Rev. D62 (2000) 114503 (hep-lat/0006022).

- [22] K. Chadan, N. N. Khuri, A. Martin and T. T. Wu, Phys. Rev. D **58** (1998) 025014 [arXiv:hep-th/9805036].
- [23] M. Li and C. I. Tan, Phys.Rev. D50 (1994) 1140-1149 [arXiv:hep-th/9401134]; M. Li and C. I. Tan, Phys. Rev. D **51** (1995) 3287 [arXiv:hep-ph/9407299].
- [24] F. E. Low, Phys. Rev. D **12** (1975) 163.
- [25] A. H. Mueller, arXiv:hep-ph/9911289.
- [26] D. Y. Ivanov, R. Kirschner, E. M. Levin, L. N. Lipatov, L. Szymanowski and M. Wusthoff, Phys. Rev. D **58** (1998) 074010 [arXiv:hep-ph/9804443].
- [27] E. Verlinde, H. Verlinde, hep-th/9302104
- [28] M. Albenese et al (APE Collaboration), Phys. Lett. B192 (1987) 163.
- [29] N. Cabibbo, E. Marinari, Phys. Lett. B119(1982) 387
- [30] K. Fabricius, O. Haan, Phys. Lett B143 (1984) 459;  
A.D. Kennedy, B.J. Pendleton, Phys. Lett., 156B (1985) 393
- [31] S.L. Adler, Phys. Rev. D 23 (1981) 2901
- [32] B. Berg and A. Billoire, Nucl. Phys. B221 (1983) 109.  
M. Lüscher, U. Wolff, Nucl. Phys. B339 (1990) 222.
- [33] M. Lüscher, private communication
- [34] V. Shevchenko and Yu. Simonov, hep-ph/0104135
- [35] H. B. Meyer, talk given at CERN, 24 April 2003
- [36] L.D. Landau, E.M. Lifshitz, “Quantum Mechanics”, 3<sup>rd</sup> ed., Pergamon Press 1977



IR	state	$\beta = 6$ $L = 16$	$\beta = 7.2$ $L = 20$	$\beta = 7.2$ $L = 40$	$\beta = 9$ $L = 24$	$\beta = 12$ $L = 32$	$\beta = 12$ $L = 42$	$\beta = 18$ $L = 50$
	$\sqrt{\sigma}$	0.2538(10)*	0.2044(5)	0.2072(46)	0.1616(6)*	0.1179(5)*	0.1179(5)*	0.0853(14)
$A_1$	$0^+$	1.198(25)	0.981(14)	0.951(14)	0.7652(78)	0.570(11)	0.577(13)	0.3970(78)
	$0^{+*}$	1.665(43)	1.396(21)	1.394(18)	1.108(23)	0.847(18)	0.839(40)	0.584(32)
	$0^{+**}$	2.198(76)	1.859(25)	1.778(34)	1.426(37)	0.980(28)	1.00(60)	0.717(76)
	$0^{+***}$	2.27(10)	2.084(41)	2.067(54)	1.522(36)	1.226(17)	1.16(12)	0.845(37)
	$4^+$	2.44(27)	2.07(33)	2.146(64)	1.570(39)	1.195(47)	1.259(98)	0.798(32)
	$4^{+*}$		2.53(13)	2.50(14)	1.700(52)	1.419(90)	1.500(48)	0.963(45)
$A_2$	$4^-$	2.54(12)	2.210(53)	2.270(64)				
$A_3$	$2^+$	1.957(48)	1.584(18)	1.567(18)	1.232(38)	0.933(11)	1.035(16)	0.634(18)
	$2^{+*}$	2.08(18)	1.870(37)	1.891(39)	1.421(44)	/	1.090(19)	0.667(20)
	$2^{+**}$	2.34(25)	2.219(90)	2.242(77)	1.660(54)	1.152(42)	1.096(92)	0.862(14)
	$2^{+***}$	2.65(29)	2.451(71)	2.47(12)	1.746(56)	1.459(29)	1.385(36)	1.019(92)
	$6^+$	2.93(21)	2.51(19)	2.64(15)	1.878(86)	1.438(28)	1.544(60)	0.906(69)
$A_4$	$2^-$	2.071(48)			1.274(37)	0.931(24)		0.643(19)
	$2^{-*}$	2.084(56)			1.359(46)	/		0.676(27)
	$2^{-**}$				1.629(59)	1.222(19)		
	$2^{-***}$				1.741(59)			
	$6^-$				1.949(64)	1.411(21)		0.952(61)

Table 1: The lightest 2+1  $SU(2)$  glueball masses on  $L^3$  lattices at the values of  $\beta$  indicated. An asterisk on the string tension indicates that the value is taken from [5].

state	$\beta = 7.2$ $L = 20$	$\beta = 9$ $L = 24$	$\beta = 12$ $L = 32$	$\beta = 18$ $L = 50$
$0^+$	1	1	1	1
$0^{+*}$	1	1	1	1
$0^{+**}$	1	1	1	/
$0^{+***}$	0.59(12)	0.68(62)	0.97(13)	1
$4^+$	0.94(9)	0.98(4)	0.38(2)	0.95(2)
$4^{+*}$	/	0.67(16)	0.59(4)	0.98(3)
$2^+$	1	1	1	
$2^{+*}$	1	1	1	
$2^{+**}$	1	1	0.97(11)	
$2^{+***}$	1	1	1	
$6^+$	/	0.87(8)	0.88(4)	

Table 2: The Fourier coefficients of the spin  $J$  states given in table 1:  $|c_J|^2$  at  $\beta = 7.2, 9, 12$  and  $18$ . When the coefficient is larger than  $0.99$ , we round it off to  $1$ .

state	$m/\sqrt{\sigma}$	conf. lev.	nb. of $\beta$
$0^+$	4.80(10)	78	5
$0^{+*}$	7.22(24)	64	4
$0^{+**}$	8.47(30)	17	5
$0^{+***}$	11.15(45)	14	3
$4^+$	9.75(45)	71	5
$4^{+*}$	12.06(88)	29	3
$2^+$	7.85(15)	50	5
$2^{+*}$	7.90(25)	15	5
$2^{+**}$	10.00(33)	32	5
$2^{+***}$	13.90(71)	35	3
$6^+$	12.09(40)	38	5

Table 3: The lightest  $2+1$   $SU(2)$  glueball masses in the continuum limit.

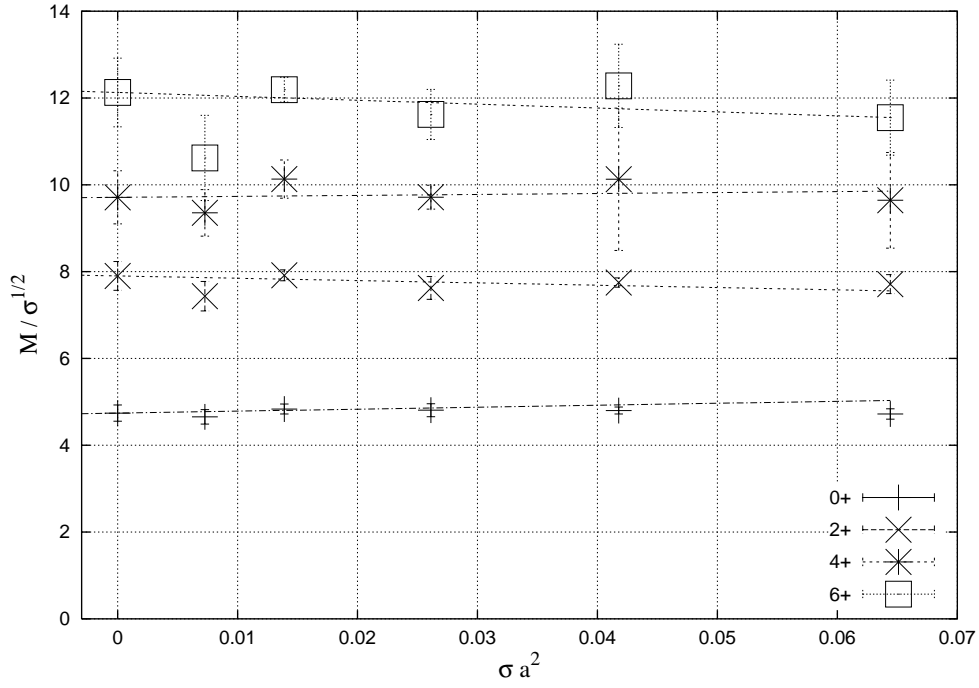


Figure 1: The continuum extrapolation of the lightest 2+1  $SU(2)$  glueball in the  $0^+$ ,  $2^+$ ,  $4^+$  and  $6^+$  sectors. The points at  $a^2\sigma = 0$  represent the result of the continuum extrapolation.

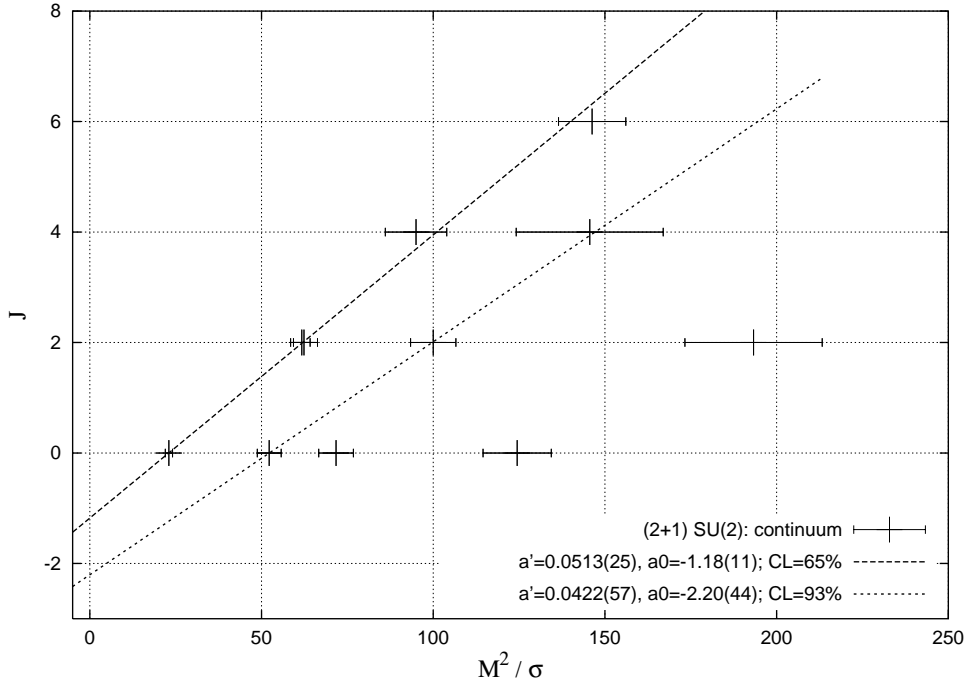


Figure 2: The Chew-Frautschi plot of the continuum 2+1  $SU(2)$  glueball spectrum

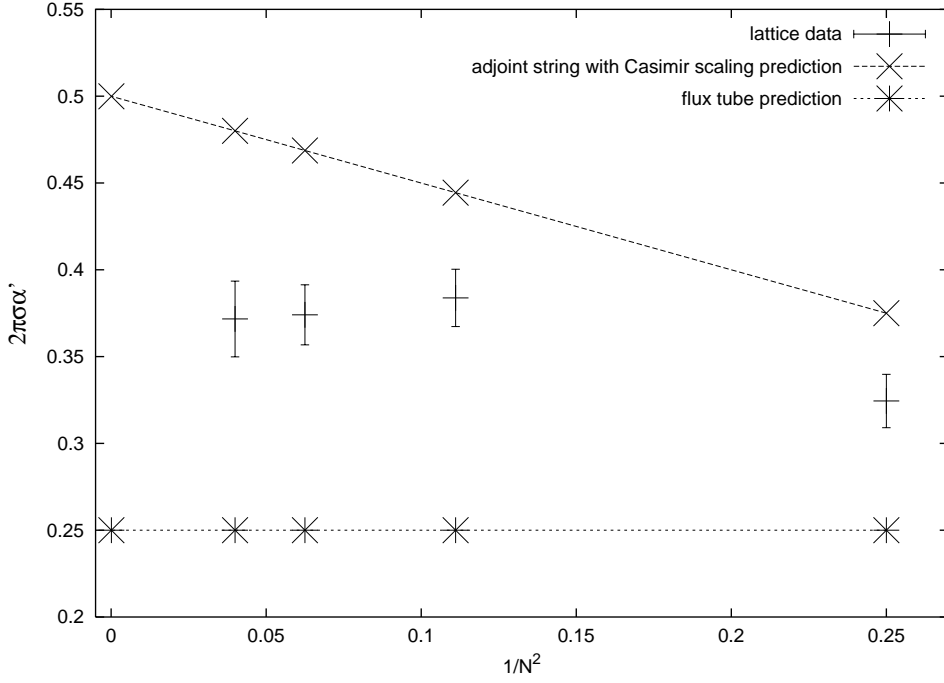


Figure 3: The slope  $\alpha'$  of the leading Regge trajectory in 2+1  $SU(N)$  gauge theory, in units of  $\frac{1}{2\pi\sigma}$ , as a function of  $\frac{1}{N^2}$

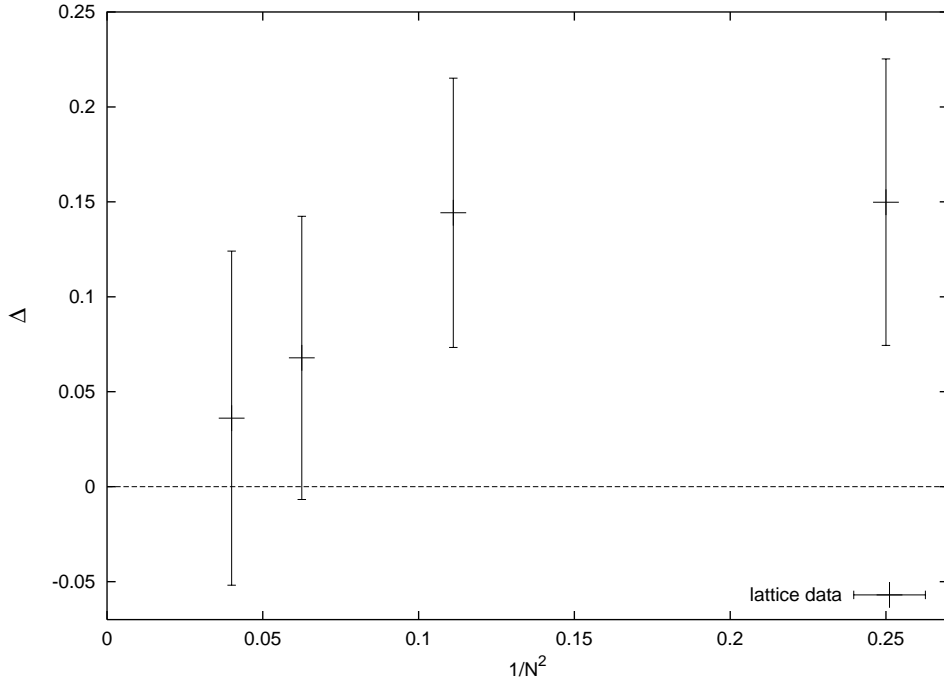


Figure 4: The difference  $\Delta \equiv -(\alpha_0 + 1)$  of the intercept to the value -1, as a function of  $\frac{1}{N^2}$  in 2+1  $SU(N)$  gauge theory